



UNIVERSITY OF LEEDS

This is a repository copy of *Influence of TiO₂-based photocatalytic coating road on traffic-related NO_x pollutants in urban street canyon by CFD modeling*.

White Rose Research Online URL for this paper:

<https://eprints.whiterose.ac.uk/161108/>

Version: Accepted Version

Article:

Xie, X, Hao, C, Huang, Y orcid.org/0000-0002-1220-6896 et al. (1 more author) (2020) Influence of TiO₂-based photocatalytic coating road on traffic-related NO_x pollutants in urban street canyon by CFD modeling. *Science of The Total Environment*, 724. 138059. ISSN 0048-9697

<https://doi.org/10.1016/j.scitotenv.2020.138059>

© 2020 Elsevier B.V. All rights reserved. This manuscript version is made available under the CC-BY-NC-ND 4.0 license <http://creativecommons.org/licenses/by-nc-nd/4.0/>

Reuse

This article is distributed under the terms of the Creative Commons Attribution-NonCommercial-NoDerivs (CC BY-NC-ND) licence. This licence only allows you to download this work and share it with others as long as you credit the authors, but you can't change the article in any way or use it commercially. More information and the full terms of the licence here: <https://creativecommons.org/licenses/>

Takedown

If you consider content in White Rose Research Online to be in breach of UK law, please notify us by emailing eprints@whiterose.ac.uk including the URL of the record and the reason for the withdrawal request.



eprints@whiterose.ac.uk
<https://eprints.whiterose.ac.uk/>

1 **Influence of TiO₂-based photocatalytic coating road on traffic-related**
2 **NO_x pollutants in urban street canyon by CFD modeling**

3 *Xiaomin Xie*1, Chenrui Hao1, Yue Huang2, Zhen Huang1,*

4 1 Key Laboratory for Power machinery and Engineering of M. O. E., Shanghai Jiao
5 Tong University, No. 800, Dongchuan Road, 200240 Shanghai, P R China

6 2 Institute for Transport Studies, University of Leeds, 34-40 University Road, Leeds,
7 LS2 9JT, UK

8

9 **ABSTRACT**

10 The use of titanium dioxide (TiO₂) photocatalytic nanoparticles as road coating to trap
11 and decompose air pollutants provides a promising technology to mitigate the harmful
12 effects of vehicle emissions. However, there are few studies on computational fluid
13 dynamics (CFD) simulations of the effect of NO_x photocatalytic oxidation in street
14 canyon with TiO₂ nanoparticles as pavement coating. This study developed a CFD
15 model with photocatalytic oxidation (PCO) reaction implemented for numerical
16 simulation of NO_x abatement in an urban street canyon with TiO₂ coating, considering
17 the effects of relative humidity (*RH*) (10–90%) and irradiance (10–40 W · m⁻²). Results
18 show that TiO₂ coating road can effectively reduce nitrogen oxide (NO_x) concentration
19 in the street canyon. The average nitric oxide (NO) and nitrogen dioxide (NO₂)
20 concentrations in street canyon with TiO₂ coating road were reduced by 3.70% and
21 4.31%, respectively, comparing with street canyon without TiO₂ coating. The irradiance

22 and relative humidity had great effect on PCO reaction in street canyon with TiO₂
23 coating road. When the irradiance increased from $10\text{ W}\cdot\text{m}^{-2}$ to $40\text{ W}\cdot\text{m}^{-2}$, average NO
24 conversion rose from 1.35% to 3.70%, and average NO₂ conversion rose from 2.43%
25 to 4.31%. The average conversion of NO and NO₂ decreased from 5.11% to 2.54% and
26 from 5.60% to 3.25%, respectively, when the relative humidity varied from 10% to 90%.
27 Results are useful to transport planners and road engineers who need to reduce NO_x
28 concentrations in urban streets travelled by fossil fuel-powered vehicles. Method of the
29 study can be considered by future research faced with different pavement construction
30 and traffic environment.

31 **Keywords:** Street canyon; TiO₂ coating road; NO_x concentration; photocatalytic
32 oxidation (PCO); computational fluid dynamics (CFD) simulation

34 1. Introduction

35 The total NO_x emissions were 12.59 Mt in China in 2017 (National Bureau of
36 Statistics of China, 2019). Vehicle exhaust is a major contributor to NO_x emissions in
37 cities with the rapidly growing automobile industry and urbanization. These activities
38 yielded an increase of 1.4 Mt NO_x in 2017 compared with the 2010 levels, while
39 pollution control measures have yielded reductions of 1.3 Mt NO_x (Zheng et al., 2018).
40 In 2017, NO_x emissions from vehicles were estimated to be 5.74 Mt (National Ministry
41 of Ecology and Environment of China, 2018), accounting for 45.6% of the total NO_x

42 emissions in China. NO_x cause a wide range of environmental issues, such as the
43 formation of tropospheric ozone and urban smog through photochemical reactions with
44 hydrocarbons. Furthermore, NO_x can cause acute respiratory tract infections and
45 cardiovascular diseases (Notario et al., 2012). Road pavement, in initial and direct
46 contact with tailpipe emissions, provides an opportunity to retain and convert the
47 pollutants to less harmful substances. Photocatalytic oxidation (PCO) is found effective
48 in reducing air pollution caused by NO_x . PCO using TiO_2 has drawn public attention
49 for air quality reasons with their advantages of high oxidation efficiency, innocuity and
50 low cost (Jiang et al., 2019).

51 Photocatalytic concrete coated with TiO_2 are widely experimented (Devahasdin et
52 al., 2003; Faraldos et al., 2016). Lasek et al. (2013) summarized the oxidation
53 mechanism, various processes and conditions of PCO for NO_x removal. Mothes et al.
54 (2018) assessed the photocatalytic performance of cement-based materials containing
55 TiO_2 for NO_x reduction, by determining the kinetic parameters under various
56 experimental conditions (relative humidity, flow rate, mixing ratio and light intensity)
57 in small-scale bed flow photoreactor experiments. Some key physic-chemical factors
58 influencing the effectiveness of photocatalytic concrete are tested in experiments by
59 (Macphee and Folli, 2016; Yang et al., 2019) on a micro level. Mendoza et al. (2017)
60 investigated the effectiveness of surface modified by WO_3/TiO_2 (WO_3 , tungsten
61 trioxide) composite particles in removing gaseous NO_x under visible light irradiation.
62 Study by Guo et al. (2017) was focusing on the method of applying nano- TiO_2 to

63 concrete surface. Based on Langmuir-Hinshelwood kinetics equation, the PCO reaction
64 rate was modelled in experiments (Ballari et al., 2010). In other experiments, the
65 reaction rate was fixed considering relative humidity and irradiance (Devahasdin et al.,
66 2003; Lira et al., 2018; Yu et al., 2010).

67 In addition to concrete, experiments were also carried out on asphalt pavement (Chen
68 and Chu, 2011)(Folli et al., 2015). De Melo et al. (2012) tested road pavement overlaid
69 with cement mortar which contains varying levels of TiO₂ (3%, 6% and 10%) for their
70 photocatalytic efficiency. Results indicated that higher TiO₂ contents in a porous
71 pavement surface are more efficient in the degradation of NO_x. Fan et al. (2018)
72 developed a solar photocatalytic asphalt for removing vehicular NO_x and mitigating
73 roadside air pollution problem by chamber tests and field tests, who studied material
74 characterizations and evaluated the durability of the photocatalytic coating.

75 The use of TiO₂ photocatalytic nanoparticles as a road coating to trap and
76 decompose air pollutants provides a promising technology to mitigate the harmful
77 effects of vehicle emissions. Certain types of urban street layouts are known to be
78 detrimental to the dispersion of contaminants. One of the typical configurations for
79 gathering pollutants and causing harm to humans is the so-called street canyon, which
80 means a street flanked by continuous buildings on both sides. Investigations on the
81 characteristics of vehicle emissions dispersion in street canyon with TiO₂ photocatalytic
82 nanoparticles as pavement coating are very important for further understanding the
83 impact of TiO₂ photocatalytic nanoparticles pavement coating on the air quality in

84 urban environment.

85 Computational fluid dynamics (CFD) simulation is used to predict the dispersion
86 of reactive air pollutants within a street canyon, because it is quick and cost effective
87 comparing with photoreactor experiment and field measurements. Baker et al. (2004)
88 and Kikumoto and Ooka (2012) simulated the dispersion and transport of reactive air
89 pollutants (NO, NO₂ and O₃) in an urban street canyon using an LES model. Kwak et
90 al. (2013) conducted numerical simulations with a Reynolds Averaged Naviere Stokes
91 equation (RANS) model to analyze the impact of bottom heating in street canyons on
92 the flow and transport of reactive air pollutants (NO, NO₂ and O₃). Heat intensity,
93 inflow wind and vegetation were found important factors that effect on reactive
94 pollution dispersion in urban street canyon (Xie and Zhu, 2018) (Moradpour et al.,
95 2017). CFD techniques are effective tools for the simulation of reactive flow within
96 photocatalytic devices considering all the coupled phenomena taking place (Lira et al.,
97 2018). CFD has been used to model flat plate photo reactor (Passalía et al., 2011)
98 (Salvado, 2007) (Salvado and Hargreaves, 2007), multi-tube reactor (Jelle Roegiers,
99 2018) (Alpert et al., 2010), impeller reactor (Tokode et al., 2017) and rectangular reactor
100 (Einaga et al., 2015). The effects of film thickness (Vezzoli et al., 2013) and gas flow
101 rate (Alpert et al., 2010) (Einaga et al., 2015) have also been investigated. However,
102 there are few studies on CFD simulations of the effect of NO_x photocatalytic oxidation
103 in street canyon with TiO₂ photocatalytic nanoparticles as pavement coating.

104 This paper aims to develop a coupled CFD-PCO model and investigate the effects of

105 TiO₂-based photocatalytic road coating on the NO_x reduction in urban street canyon.
106 Furthermore, a comprehensive analysis of the key factors influencing the effectiveness
107 of the TiO₂-based photocatalytic coating road is carried out. Methodology in this study
108 will provide a fast and effective way for the investigation of the PCO reaction in street
109 canyon with TiO₂ coating road. Findings from this study shall be useful to road design
110 and transport planning to reduce reactive pollutant levels in urban traffic environment.

111 **2. Methodology**

112 **2.1 Flow modeling**

113 Computational fluid dynamics (CFD) modelling is based on numerical solutions to
114 derive dispersion equations and fluid flow simulation. These solutions are derived from
115 the principles of conservation and transmission. The air in street canyons can be
116 considered incompressible turbulent inert flow, and the density of air and pollutant is
117 assumed to be constant. As Sini et al. (1996) pointed out, these assumptions are
118 reasonable for most low-level atmospheric environments.

119 Steady RANS model has been widely used because its effectiveness in predicting
120 average airflows. Re-normalization group (RNG) $k-\varepsilon$ model is used in this study
121 according to previous research on the influence of structures on particulate matter
122 dispersion in street canyons by CFD modeling (Hao et al. 2019).

123 The commercial CFD software Fluent (Fluent, 2009) is used to implement the
124 mathematical model above. Meanwhile, the governing equations are discretized using

125 the finite volume method and the second order upwind scheme. The SIMPLE scheme
126 is used for the pressure and velocity coupling.

127 The inlet flow velocity is:

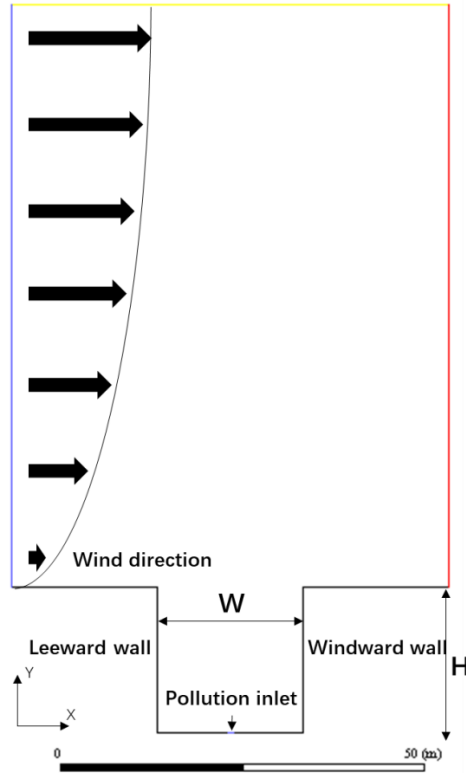
$$128 \quad u(z) = U_0 \left(\frac{y-H}{Y} \right)^\alpha \quad (1)$$

129 where U_0 is the wind speed at the boundary, it is set as $U_0 = 3 \text{ m}\cdot\text{s}^{-1}$. H is the height
130 of the building and Y is the thickness of the boundary which is set to 80 m in the paper.

131 The same thickness was also applied in Ai and Mak's simulation (Ai and Mak, 2017).

132 α is the wind profile exponent indicating the base surface roughness in relation to the
133 terrain category of mid-dense urban area, and was set to 0.22 (Hang et al., 2017).

134 Simulations in this study are performed with a full-scaled model. Fig.1 shows the
135 computational domain. The buildings' height H and street's width W are all 20 m. The
136 ratio $H/W = 1$. Pollution inlet is set in the middle of the ground with 1 m wide. The
137 domain size is 20 m by 100 m in x and y directions. Regular grids of 0.1 m by 0.1 m
138 are applied to the whole area inside the street canyon. Grid size outside the canyon
139 increases as they have less effect. Velocity-inlet is applied to the air inlet. The outlet is
140 set with outflow condition. The top domain is considered symmetrical. Walls are
141 defined as non-slip walls. Temperature is set as 298K (about 25°C) in the domain and
142 at all the walls, which means the canyons are isothermal.



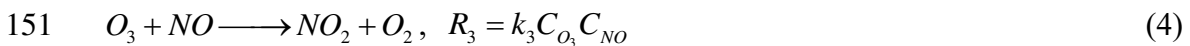
143

144

Fig.1. Computational domain

145 2.2 PCO reaction mechanism

146 A simplified photochemical steady state (PSS) O_3/NO_x model is implemented if the
 147 road is without TiO_2 coating. The chemical reactions considered are (Baik et al., 2007;
 148 Carpenter et al., 1998)



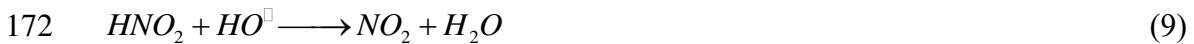
152 In Eq.(2), $h\nu$ represents photovoltaic processes triggered by sunlight. In Eq. (3),
 153 M means a third-body molecule that absorbs energy and stabilizes O_3 . Above reaction
 154 mechanism has been widely used in previous studies (García-yea et al., 2018; Han et

155 al., 2018; Muilwijk et al., 2016; Ryerson et al., 2000; Xie and Zhu, 2018).

156 The rate of Eq. (2) is considered infinitely fast compared to the photolysis rate R_1 ,
157 e.g. $k_2 \approx \infty$ (Muilwijk et al., 2016). k_1 is specified as 0.0081 s^{-1} and
158 $k_3 = 44.05 \times 10^{-3} \exp(-1370/T) \text{ ppb}^{-1} \text{ s}^{-1}$ (Baik et al., 2007; Seinfeld, 2007). Eq. 2-4 are
159 combined with the steady RANS method to simulate the dispersion of NO and NO₂.

160 In this simulation, NO and NO₂ are released from the pollution inlet (Fig.1) with a
161 mole fraction of 50 ppm and 5 ppm, respectively. The releasing speed is defined as
162 0.002m/s. It corresponds to about 1000 vehicles per hour, the emission intensity of NO
163 and NO₂ are $120.7 \mu\text{g}\cdot\text{m}^{-1}\cdot\text{s}^{-1}$ and $18.5 \mu\text{g}\cdot\text{m}^{-1}\cdot\text{s}^{-1}$, respectively, assuming the NO_x
164 emission rate is $0.5 \text{ g}\cdot\text{km} / \text{s}$ per vehicle (Baker et al., 2004).

165 Furthermore, road with nanometer TiO₂ coating is associated with the photocatalytic
166 oxidation (PCO) of nitrogen oxides in street canyon. The related reactions are written
167 below (Allen et al., 2003):



174 The Langmuir-Hinshelwood model has been widely used to model the reaction rate
175 for PCO (M. M. Ballari et al., 2010; Mills and Hunte, 1997; Muñoz et al., 2019). Ballari

176 et al. (2010) developed equations to calculate the reaction rate of NO and NO₂ for
 177 surface reactions at constant *RH* and irradiance. Lira et al. (2018) took the effects of
 178 *RH* and irradiance into account in developing the equations, which are written below:

$$179 \quad r_{NO} = -\frac{k'_{NO}C_{NO}}{1 + K_{NO}C_{NO} + K_{NO_2}C_{NO_2} + K_wC_w}(-1 + \sqrt{1 + \alpha E}) \quad (11)$$

$$180 \quad r_{NO_2} = -\frac{k'_{NO_2}C_{NO_2} - k'_{NO}C_{NO}}{1 + K_{NO}C_{NO} + K_{NO_2}C_{NO_2} + K_wC_w}(-1 + \sqrt{1 + \alpha E}) \quad (12)$$

181 where k'_i and K_i are intrinsic kinetic and equilibrium parameters, respectively. α
 182 is kinetic parameter related to irradiance and E is irradiance. The constants derived by
 183 Lira et al. (2018) are based on the values derived by Ballari et al. (2010), which are
 184 taken as reference values in this study. The values are listed in Table 2.

185 Table 2 Values adopted in Eq. (11-12) (Lira et al., 2018)

Parameter	Value	Unit
k'_{NO}	4.18	$m \cdot s^{-1}$
k'_{NO_2}	6.73	$m \cdot s^{-1}$
K_{NO}	8.48×10^8	$m^3 \cdot kmol^{-1}$
K_{NO_2}	3.02×10^8	$m^3 \cdot kmol^{-1}$
K_w	5.07×10^4	$m^3 \cdot kmol^{-1}$
α	2.37×10^{-3}	$m^2 \cdot W^{-1}$

186 Photoactive components of photocatalytic coatings are activated by ultraviolet (UV)
 187 light (de Melo and Trichês, 2012)(Guo et al., 2017)(Diamanti et al., 2013). The
 188 proportion of UV light to total radiation intensity is about 8.7% (Zhang, 2014).

189 According to the radiation intensity and RH data in different region of China (National
190 Bureau of Statistics of China, 2019), irradiance (E) varies in the range of $10-40 \text{ W} \cdot \text{m}^{-2}$,
191 RH varies in the range of 10%-90%. E of $40 \text{ W} \cdot \text{m}^{-2}$ and RH of 50% are set as the
192 reference condition in this study.

193 **2.3 Calculation for pollutant conversion**

194 In order to evaluate the effects of TiO_2 coating on the PCO reactions in street
195 canyon, pollutant conversion (X_{NO}) is defined as:

$$196 \quad X_i = \left(\frac{C_i^{\text{noPCO}} - C_i^{\text{PCO}}}{C_i^{\text{noPCO}}} \right) \times 100\% \quad (13)$$

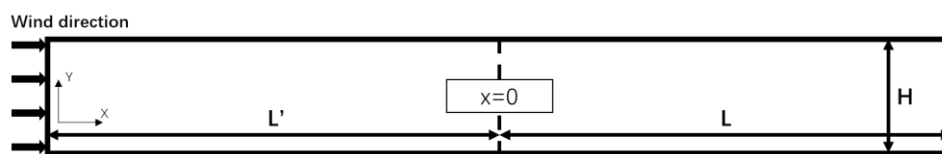
197 i stands for the type of the pollutant, here refer to NO and NO_2 . C_i^{PCO} means the
198 average pollutant concentration using the model with PCO reactions. C_i^{noPCO} means
199 the average pollutant concentration using the model without PCO reactions. The higher
200 the X_i , the more effective the PCO reaction is.

201 **3. Model validation**

202 The accuracy of the above developed CFD model was evaluated using results from
203 the wind-tunnel experiments by Allegrini et al. (2014). The validation setups for flow
204 modeling have been detailed in previous publication (Hao et al., 2019). In order to
205 validate the chemical reaction model, a 2D computational domain (Fig.2) with a length
206 ($L+L'$) of 0.4 m and a height (H) of 3 mm was built similar to Lira et al.'s study (Lira
207 et al., 2018) for comparing with Ballari et al.'s experiment (M. M. Ballari et al., 2010).

208 The domain's height uses value 2H and 4H (keeping the length constant). The bottom
 209 of the domain with length L ($0 < x < 0.2$ m) is set as a reactive surface. The reaction
 210 mechanism is written in Eq. (5-10). Domain with length L' ($0 < x < 0.2$ m) is set as a
 211 control group without PCO to obtain a fully developed laminar velocity profile at $x=0$.
 212 Inlet velocity is set to 0.1667 m/s. A concentration of $4.47 \times 10^{-8} \text{ kmol} \cdot \text{m}^{-3}$ for NO and
 213 a relative humidity of 50% is set at the inlet. A homogeneous irradiance of $10 \text{ W} \cdot \text{m}^{-2}$
 214 is imposed at the reactive surface. Simulation results are compared to those from Lira
 215 et al.'s (Lira et al., 2018) and Ballari et al.'s experiment (M. M. Ballari et al., 2010). In
 216 order to compare the experiment results between different tests, the NO conversion
 217 (X_{NO}) is specified as:

$$218 \quad X_{NO} = \left(\frac{C_{NO}^{in} - C_{NO}^{avg,out}}{C_{NO}^{in}} \right) \times 100\% \quad (14)$$

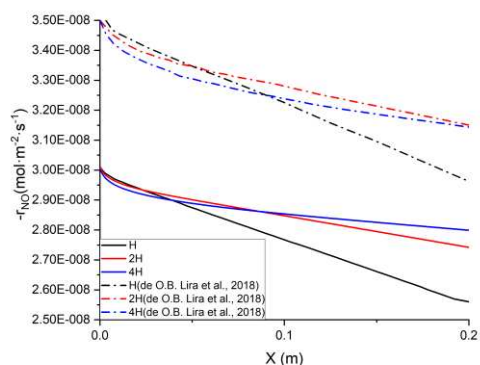


219
220 Fig.2. Computational domain for chemical reaction validation

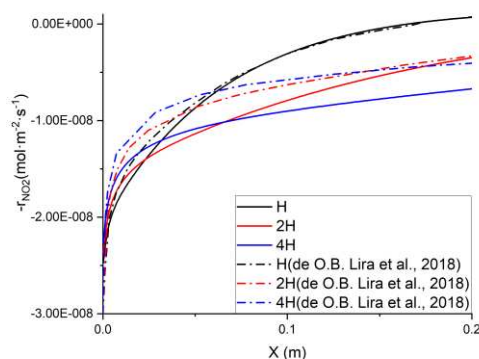
221 The results including comparison with those by Lira et al. (Lira et al., 2018) are
 222 shown in Fig.3. Fig.3(a) shows the reaction rates for NO along x-axis at the reactive
 223 surface. A gap was observed when comparing the results with Lira et al.'s. However,
 224 the tendency is the same that the rates decrease along the direction of wind. The reaction
 225 rates obtained in this study are lower than in the reference study. As a result, the profiles
 226 of NO mass fractions obtained for $0 < x < L$ (Fig.3(c)) in this study are higher than Lira
 227 et al.'s. The results for NO_2 are shown in Fig.3(b) & (d). Reaction rates of NO_2 at the

228 reactive surface show high similarity with the reference. Values of NO_2 mass fractions
 229 are higher in this study, compared to the reference.

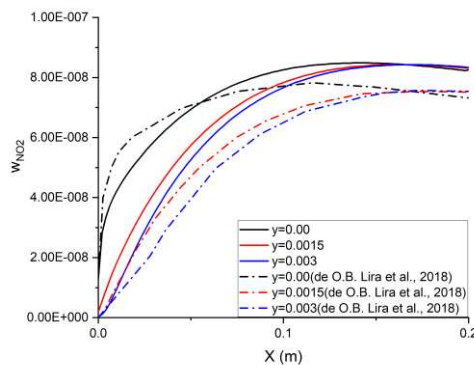
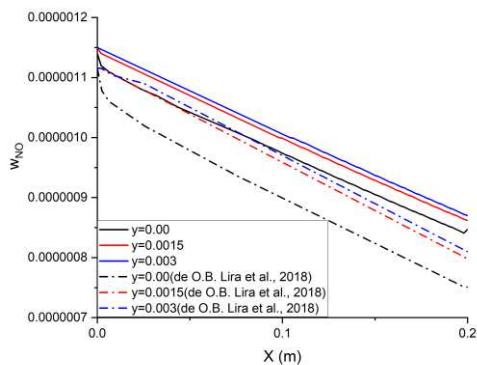
230 Results for X_{NO} in this validation comparing with reference simulation (Lira et al.,
 231 2018) and experiment (M. M. Ballari et al., 2010) are shown in Fig.4. Clearly, there is
 232 a tendency of decreasing X_{NO} as the relative humidity increases. It is worth noting that
 233 simulation in this validation matches Ballari et al.'s experiment better than Lira et
 234 al.'s study (Lira et al., 2018), although it overestimates NO conversion. After validation,
 235 the chemical mechanism model applied in this study is considered reliable for
 236 predicting the chemical reaction and transformation.



(a) Reaction rates for NO along x-axis at the reactive surface.



(b) Reaction rates for NO_2 along x-axis at the reactive surface.



(c) Profiles of NO mass fractions (d) Profiles of NO₂ mass fractions
 obtained for $0 < x < L$ at $y = 0.00, 0.0015$ obtained for $0 < x < L$ at $y = 0.00, 0.0015$
 and 0.003 m and 0.003 m

Fig.3. Comparison results with Lira et al.

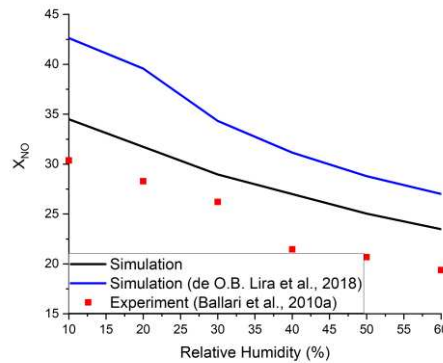


Fig.4. Comparison of NO conversion (X_{NO}) with experiment as a function of relative humidity

237 **4. Results and discussion**

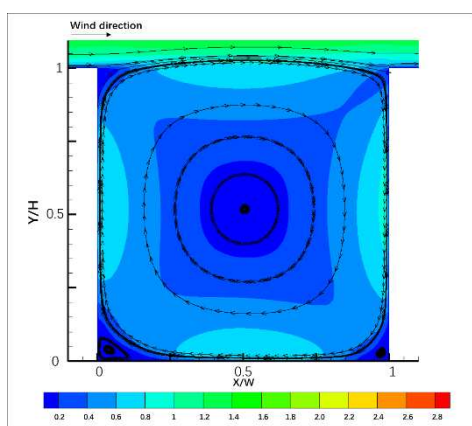
238 **4.1 NO_x dispersion in street canyon with TiO₂ coating road**

239 In this section, simulation results of a street canyon with TiO₂ coating road are
 240 compared with a street canyon without TiO₂ coating road.

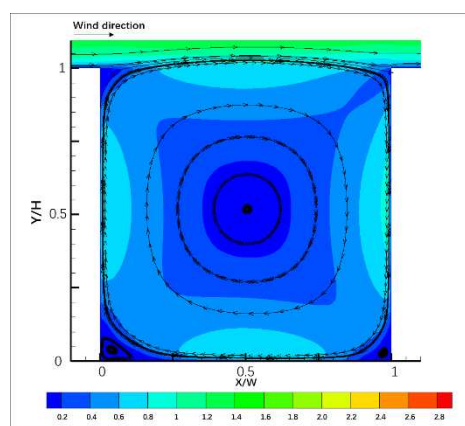
241 Fig.5 illustrates the wind flow structures and pollutant dispersion patterns in the street
 242 canyons with and without TiO₂ coating road. Due to the presence of clockwise eddy,
 243 most of the pollutants accumulated in the leeward side, as shown in Fig.5a and Fig.5b.

244 Decreases of NO concentration were observed in the street canyon with TiO₂ coating
 245 road. In details, the average concentration of NO inside the street canyon with TiO₂

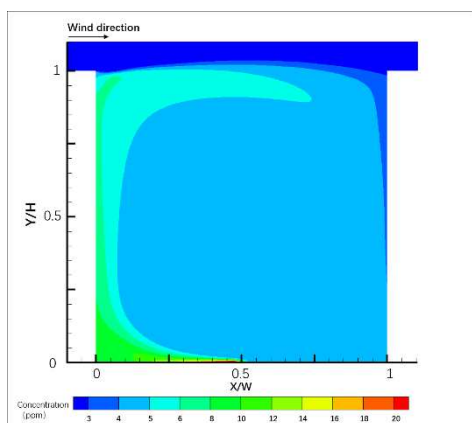
246 coating road is 6.06 ppm, while it is 6.29 ppm inside the street canyon without TiO₂
 247 coating road, as shown in Fig.5c and Fig.5d. This means the average NO concentration
 248 decreases by 3.70% under the influence of PCO reactions. Similar reduction in NO₂
 249 concentration inside the canyon is shown in Fig.5e and Fig.5f. The PCO decreases the
 250 average concentration of NO₂ by 4.31%.



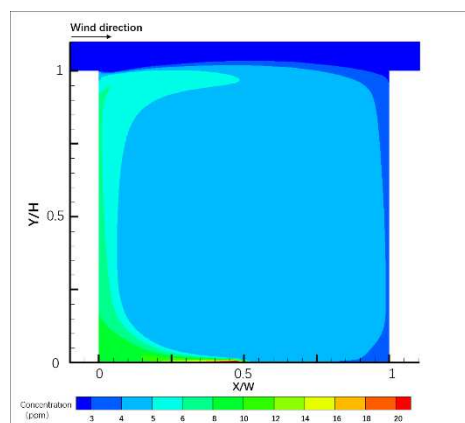
(a) Flow field and velocity contour in canyon without TiO₂ coating road.



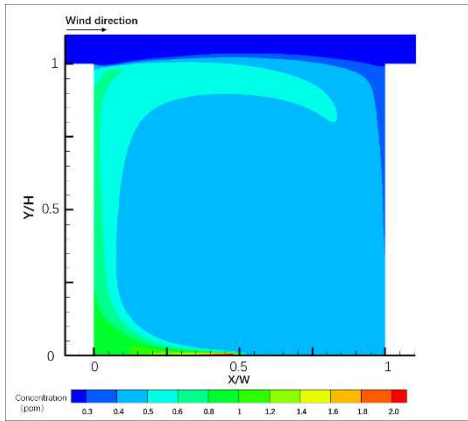
(b) Flow field and velocity contour in canyon with TiO₂ coating road.



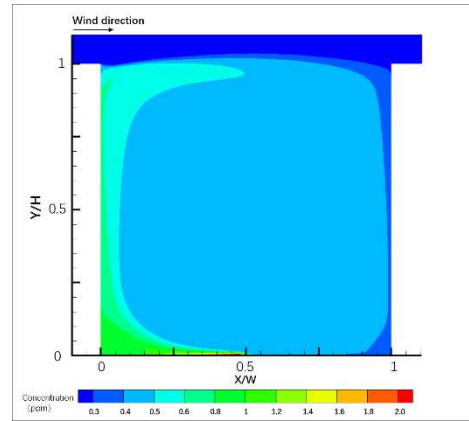
(c) Contour of NO concentration in canyon without TiO₂ coating road.



(d) Contour of NO concentration in canyon with TiO₂ coating road.



(e) Contour of NO₂ concentration in canyon without TiO₂ coating road.

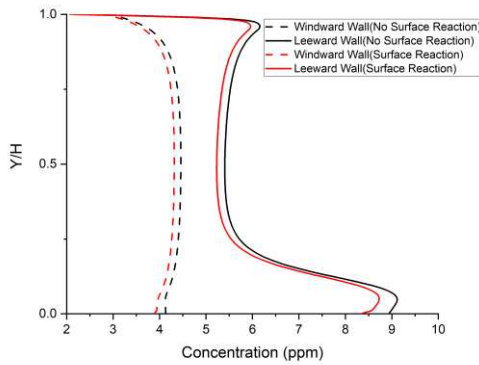


(f) Contour of NO₂ concentration in canyon with TiO₂ coating road.

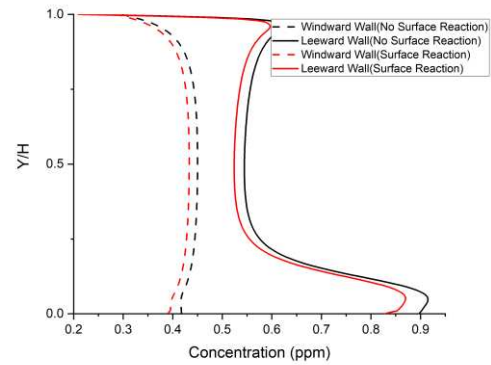
Fig.5 Flow fields, contours of flow velocity and NO_x concentration in the observed street canyons.

251 Profiles of NO and NO₂ concentration at the leeward wall, windward wall and the
 252 breathing zone are shown in Fig.6. The breathing zone is defined as a height of y=1.5
 253 m because it is about the nose height of the pedestrians. Concentrations at leeward and
 254 windward wall can influence the health of people who live or work in the buildings on
 255 either side of the street. It is obvious that the NO_x concentration is lower in street
 256 canyons with TiO₂ coating road in all observed profiles. The average NO and NO₂
 257 concentration at the height of breathing zone decrease by 3.29% and 3.88%,
 258 respectively, under the influence of PCO reactions. The average NO concentration near
 259 the windward wall and leeward wall decrease by 3.28% and 3.35%, respectively. The
 260 average NO₂ concentration near the windward wall and leeward wall decrease by 3.84%
 261 and 3.95%, respectively. Conclusions can thus be drawn that the PCO reactions with
 262 TiO₂ coating decrease the NO_x concentration inside street canyon. However, the
 263 characteristics of pollutant profiles are similar for street canyons with and without TiO₂

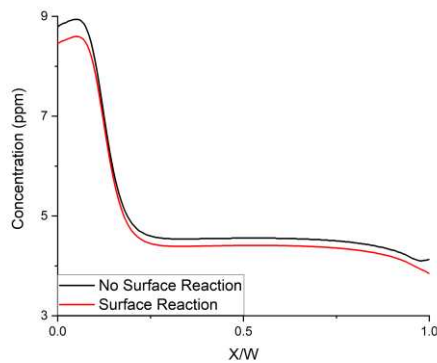
264 coating road. NO and NO₂ concentrations at windward wall reach high level at
 265 0.25H<y<0.75H. Conversely, NO and NO₂ concentrations at leeward wall at
 266 0.25H<y<0.75H are at a low level, while reaching the peak value at about y=0.05H.
 267 NO and NO₂ concentrations at breathing zone have the peak value near leeward wall
 268 (x<~0.2W). That means pedestrians near the leeward side are exposed to more pollution
 269 than at the windward side. PCO reaction with TiO₂ coating can lead to 3-4% reduction
 270 of NO and NO₂ in this area.



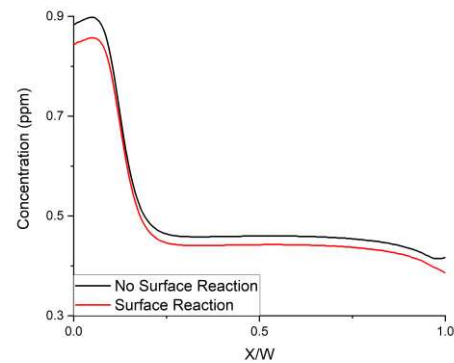
(a) Profiles of NO concentration at leeward and windward wall along $0 < y < H$



(b) Profiles of NO₂ concentration at leeward and windward wall along $0 < y < H$



(c) Profiles of NO concentration at the breathing zone along $0 < x < W$

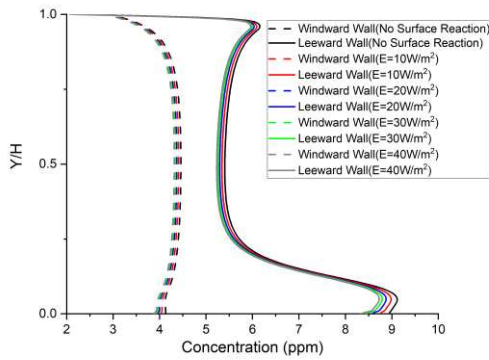


(d) Profiles of NO₂ concentration at the breathing zone along $0 < x < W$

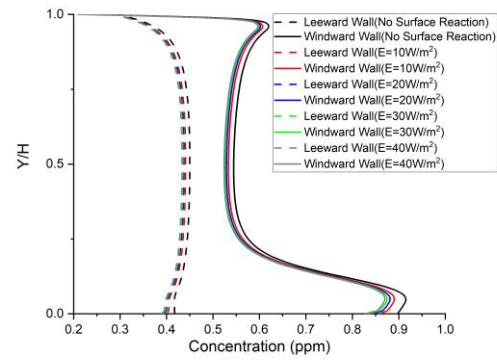
Fig.6 Profiles of NO and NO₂ concentration.

271 4.2 Effects of irradiance on PCO and NO_x profiles

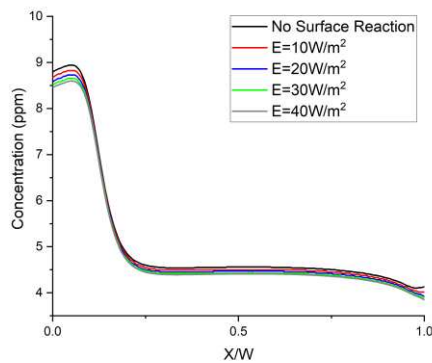
272 Irradiance (E) is varied in the range of 10-40 $W \cdot m^{-2}$ when analysing the effects of
273 irradiance on the PCO and NO_x profiles in street canyon. The relative humidity (50%)
274 is kept constant. Fig.7 shows the profiles of NO and NO₂ concentration in relation to
275 irradiance. At leeward wall, the peak value of NO_x concentration is at $\sim 0.05H$. The peak
276 value decreases from 9.11ppm to 8.7ppm for NO, and from 0.92ppm to 0.87ppm for
277 NO₂, when irradiance increase from 0 to 40 $W \cdot m^{-2}$. The reductions of NO and NO₂
278 concentration are 4.5% and 5.4%, respectively. There is a sharp decrease along
279 $0.05H < y < 0.25H$. The NO_x concentration near the roof of the leeward building has a
280 small spike, reaching about 6 and 0.6 ppm for NO and NO₂, respectively. At windward
281 wall, the concentration is in constant change and much lower than the leeward wall. In
282 the breathing zone, the peak value of NO concentration is at about $x=0.1W$ and ranges
283 from 8.5~9 ppm with varied irradiance. The concentration falls rapidly along
284 $0.1W < x < 0.2W$. The reaction rates of NO and NO₂ are monotonic functions of the
285 irradiance (E), i.e. the increase of irradiance accelerates the reaction. NO and NO₂
286 concentrations in street canyon decrease when the irradiance increase.



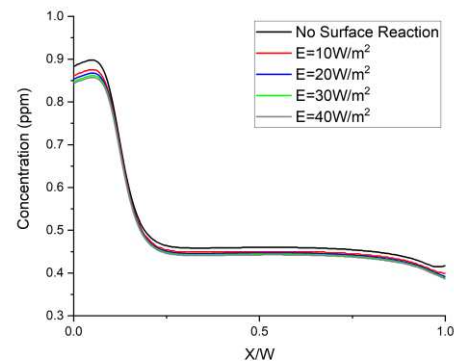
(a) Profiles of NO concentration at leeward and windward wall along $0 < y < H$



(b) Profiles of NO₂ concentration at leeward and windward wall along $0 < y < H$



(c) Profiles of NO concentration at the breathing zone along $0 < x < W$

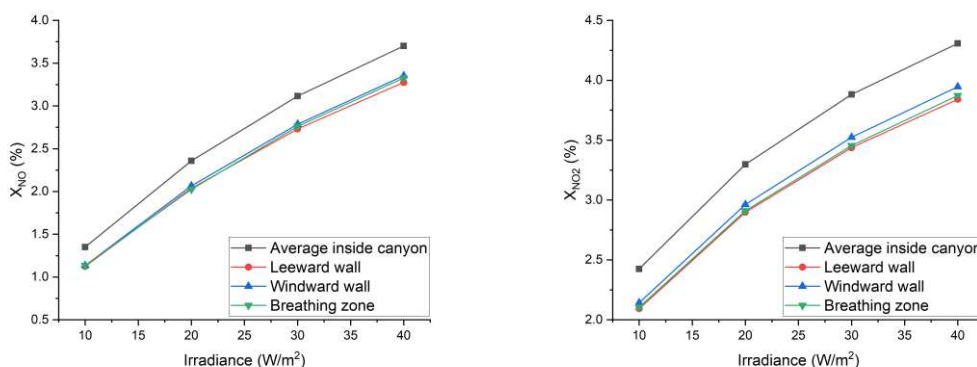


(d) Profiles of NO₂ concentration at the breathing zone along $0 < x < W$

Fig.7 Profiles of NO and NO₂ concentration in conditions with varied irradiance.

287 Fig.8 presents the NO and NO₂ conversions. For both NO and NO₂, the conversion
 288 increases when the irradiance increases. The conversion at leeward wall, windward wall
 289 and breathing zone is similar. However, the average conversion of pollutants inside the
 290 whole street canyon is higher than all three zones. The PCO reaction happens on the
 291 ground while air flow still carries more pollutants to the ground and the buildings'

292 external surfaces. This explains why the NO_x is absorbed by the TiO_2 coating road but
 293 the lowest NO_x conversion is not at the breathing zone which is near the ground.
 294 Average conversions of NO and NO_2 in street canyon reduce from 3.70% to 1.35% and
 295 from 4.31% to 2.43%, respectively, when the irradiance decreases from $40 \text{ W} \cdot \text{m}^{-2}$ to
 296 $10 \text{ W} \cdot \text{m}^{-2}$. It can be seen that the irradiance has a great effect on PCO reaction in a
 297 street canyon with TiO_2 coating road. The higher the irradiance, the more effective the
 298 PCO reaction is. The NO_2 conversion is always higher than NO , which means NO_2 is
 299 more sensitive to PCO reaction in the conditions set in this study.
 300



(a) NO conversion (X_{NO}) as a function of the irradiance. (b) NO_2 conversion (X_{NO_2}) as a function of the irradiance.

Fig.8 Pollutant conversion as a function of the irradiance.

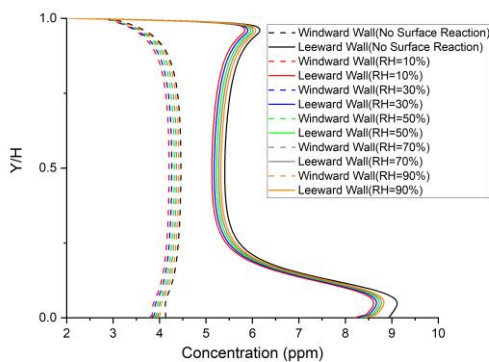
301 4.3 Effects of relative humidity on PCO and NO_x profiles

302 The effect of relative humidity on PCO and pollutant concentration in a street canyon
 303 with TiO_2 coating road is studied by changing the relative humidity (RH) in the range

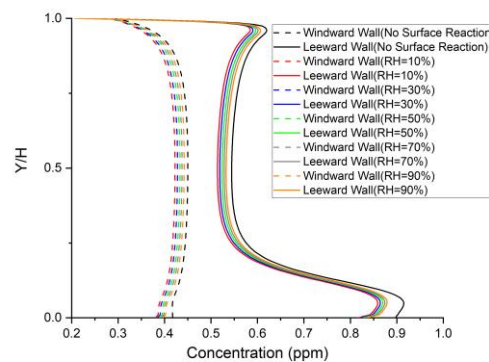
304 of 10-90%. The irradiance ($40 W \cdot m^{-2}$) is kept constant. Profiles of NO and NO₂
305 concentration at leeward and windward are shown in Fig.9 (a) and (b). It can be seen
306 that the characteristics of pollutant distribution along the walls are consistent with the
307 relative humidity. At leeward wall, the peak value of NO and NO₂ concentration is at
308 $x \sim 0.05H$, and the maximum rising rate is 2.5% (NO) and 1.7% (NO₂) when relative
309 humidity increases from 10% to 90%. NO and NO₂ concentration at the windward side
310 increase more when the relative humidity increases, comparing with that at the leeward
311 side, which see an increase of 5% (NO) and 3% (NO₂) when relative humidity increases
312 from 10% to 90%. NO and NO₂ concentration profiles at the breathing zone is shown
313 in Fig.9 (c)-(d). The NO and NO₂ concentration at the breathing zone rise from 2.6%
314 to 5.3% and from 2.3% to 5.3%, respectively, when relative humidity increases from
315 10% to 90%. Lower relative humidity results in more effective PCO reaction and lower
316 NO_x concentration in street canyon.

317 Fig.10 shows the effect of relative humidity on NO_x conversion. It is clear that when
318 the relative humidity increases, the NO and NO₂ conversions decrease in street canyon.
319 The same tendency can be also seen from conversions at the leeward wall, windward
320 wall and breathing zone. However, the change rates in different locations are different.
321 The average conversion of the whole street canyon is higher than the three zones when
322 relative humidity is 50%-90%. The gap between the average conversion of the whole
323 canyon and the zones gets narrower when the relative humidity decreases. When the
324 relative humidity is 30%, the conversions of the four computational domains (whole

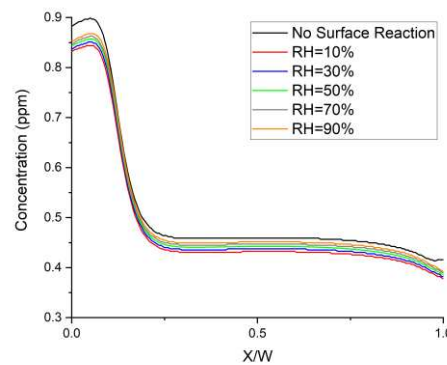
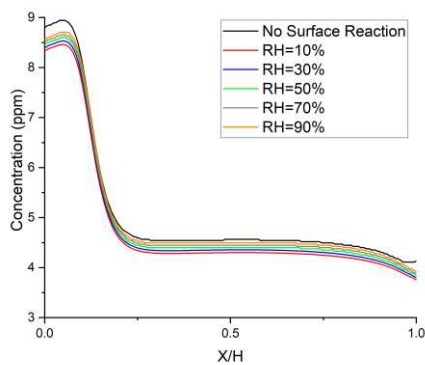
325 street canyon, leeward wall, windward wall and breathing zone) are similar. Average
 326 conversion of NO and NO₂ in street canyon decrease from 5.11% to 2.54% and from
 327 5.60% to 3.25%, respectively, when the relative humidity increase from 10% to 90%.
 328 Within the pollutant accumulated zone, NO and NO₂ conversion at leeward wall have
 329 the greatest change with the same change of relative humidity. Along the leeward wall,
 330 the highest NO and NO₂ conversions are 5.77% and 5.23%, respectively, when
 331 $RH=10\%$, and the lowest NO and NO₂ conversions are 1.17% and 1.71%, respectively,
 332 when $RH=90\%$.



(a) Profiles of NO concentration at leeward and windward wall along $0 < y < H$

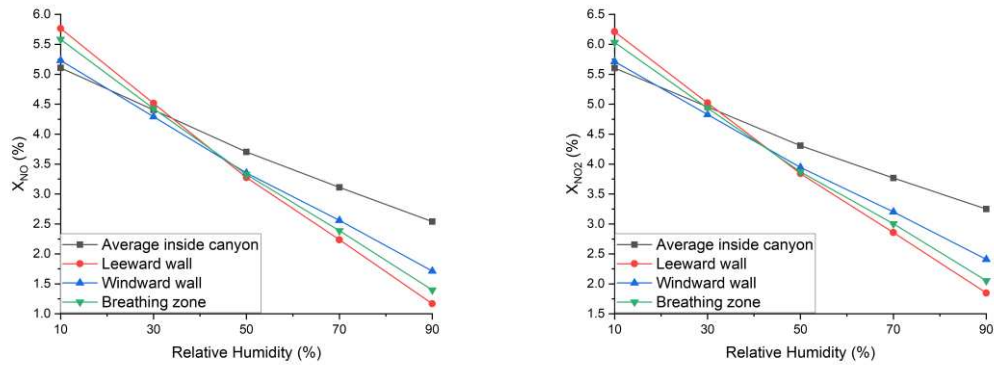


(b) Profiles of NO₂ concentration at leeward and windward wall along $0 < y < H$



(c) Profiles of NO concentration at the breathing zone along $0 < x < W$ (d) Profiles of NO₂ concentration at the breathing zone along $0 < x < W$

Fig.9 Profiles of NO and NO₂ concentration in conditions with varied relative humidity.



(a) NO conversion (X_{NO}) as a function of the relative humidity. (b) NO₂ conversion (X_{NO2}) as a function of the relative humidity.

Fig.10 Pollutant conversion as a function of the relative humidity.

333 5. Conclusions and recommendations

334 A CFD model coupled with PCO reaction is implemented and validated with
 335 experimental data available in the literature for NO_x abatement in a real urban street
 336 canyon with aspect ratio $H/W=1$. Irradiance and relative humidity are investigated, as
 337 the factors that can influence the behavior of the TiO₂ coating road with a representative
 338 TiO₂ concrete characteristic . Results show that TiO₂ coating road can effectively reduce
 339 NO_x concentration in the street canyon. The irradiance and the relative humidity have
 340 great effect on PCO reaction and on reducing the NO_x concentration in street canyon

341 with TiO₂ coating road. The higher the irradiance, the more effective the PCO reaction
342 is. When the relative humidity is increased, the NO and NO₂ conversions tend to
343 decrease.

344 CFD model implemented in this study can be readily used for the investigation of
345 PCO reaction in street canyon with TiO₂ coating road. Different influencing factors can
346 be investigated using the model, allowing for fast and effective preliminary evaluation
347 of several scenarios aiming at the photocatalytic process. According to experiment
348 studies (Faraldos et al., 2016; Fresno et al., 2014; Lasek et al., 2013), the behavior of
349 TiO₂ concrete is related to the type of TiO₂ concrete and the concentration of TiO₂. For
350 further studies, different types of TiO₂ concrete can be tested and evaluated. Other
351 applications of TiO₂ coating may also be modeled and evaluated, for example, TiO₂
352 paint coated on building facades.

353

354 **ACKNOWLEDGEMENTS**

355 The work described in this paper was financially supported by National Natural
356 Science Foundation of China (No.50808124).

357

358 **References**

359 Ai, Z.T., Mak, C.M., 2017. CFD simulation of flow in a long street canyon under a

360 perpendicular wind direction: Evaluation of three computational settings.
361 Building and Environment 114, 293–306.
362 <https://doi.org/10.1016/j.buildenv.2016.12.032>

363 Allegrini, J., Dorer, V., Carmeliet, J., 2014. Buoyant flows in street canyons:
364 Validation of CFD simulations with wind tunnel measurements. Building and
365 Environment 72, 63–74. <https://doi.org/10.1016/j.buildenv.2013.10.021>

366 Allen, G., Janes, P., Nicholson, J., Dalton, J., Jones, N., Hallam, K., 2003.
367 Photocatalytic oxidation of NO_x gases using TiO₂: a surface spectroscopic
368 approach. Environmental Pollution 120, 415–422. [https://doi.org/10.1016/s0269-](https://doi.org/10.1016/s0269-7491(02)00107-0)
369 [7491\(02\)00107-0](https://doi.org/10.1016/s0269-7491(02)00107-0)

370 Alpert, S.M., Knappe, D.R.U., Ducoste, J.J., Blvd, P.P., 2010. Modeling the UV /
371 hydrogen peroxide advanced oxidation process using computational fluid
372 dynamics. Water Research 44, 1797–1808.
373 <https://doi.org/10.1016/j.watres.2009.12.003>

374 Baik, J.J., Kang, Y.S., Kim, J.J., 2007. Modeling reactive pollutant dispersion in an
375 urban street canyon. Atmospheric Environment 41, 934–949.
376 <https://doi.org/10.1016/j.atmosenv.2006.09.018>

377 Baker, J., Walker, H.L., Cai, X., 2004. A study of the dispersion and transport of
378 reactive pollutants in and above street canyons - A large eddy simulation.
379 Atmospheric Environment 38, 6883–6892.
380 <https://doi.org/10.1016/j.atmosenv.2004.08.051>

381 Ballari, Hunger, Hüsken, HBrouwers, 2010. NO_x photocatalytic degradation
382 employing concrete pavement containing titanium dioxide. *Applied Catalysis B:
383 Environmental* 95, 245–254. <https://doi.org/10.1016/j.apcatb.2010.01.002>

384 Ballari, M.M., Hunger, M., Hüsken, G., Brouwers, H.J.H., 2010. Modelling and
385 experimental study of the NO_x photocatalytic degradation employing concrete
386 pavement with titanium dioxide *151*, 71–76.
387 <https://doi.org/10.1016/j.cattod.2010.03.042>

388 Carpenter, L.J., Clemitshaw, K.C., Burgess, R.A., Penkett, S.A., Cape, J.N.,
389 McFadyen, G.G., 1998. Investigation and evaluation of the NO(x)/O₃
390 photochemical steady state. *Atmospheric Environment* 32, 3353–3365.
391 [https://doi.org/10.1016/S1352-2310\(97\)00416-0](https://doi.org/10.1016/S1352-2310(97)00416-0)

392 Chen, M., Chu, J.W., 2011. NO_x photocatalytic degradation on active concrete road
393 surface - From experiment to real-scale application. *Journal of Cleaner
394 Production* 19, 1266–1272. <https://doi.org/10.1016/j.jclepro.2011.03.001>

395 de Melo, J.V.S., Trichês, G., 2012. Evaluation of the influence of environmental
396 conditions on the efficiency of photocatalytic coatings in the degradation of
397 nitrogen oxides (NO_x). *Building and Environment* 49, 117–123.
398 <https://doi.org/10.1016/j.buildenv.2011.09.016>

399 De Melo, J.V.S., Trichês, G., Gleize, P.J.P., Villena, J., 2012. Development and
400 evaluation of the efficiency of photocatalytic pavement blocks in the laboratory
401 and after one year in the field. *Construction and Building Materials* 37, 310–319.

402 <https://doi.org/10.1016/j.conbuildmat.2012.07.073>

403 Devahasdin, S., Fan, C., Li, K., Chen, D.H., 2003. TiO₂ photocatalytic oxidation of
404 nitric oxide: Transient behavior and reaction kinetics. *Journal of Photochemistry
405 and Photobiology A: Chemistry* 156, 161–170. [https://doi.org/10.1016/S1010-
406 6030\(03\)00005-4](https://doi.org/10.1016/S1010-6030(03)00005-4)

407 Diamanti, M. V., Del Curto, B., Ormellese, M., Pedferri, M.P., 2013. Photocatalytic
408 and self-cleaning activity of colored mortars containing TiO₂. *Construction and
409 Building Materials* 46, 167–174.
410 <https://doi.org/10.1016/j.conbuildmat.2013.04.038>

411 Einaga, H., Tokura, J., Teraoka, Y., Ito, K., 2015. Kinetic analysis of TiO₂-catalyzed
412 heterogeneous photocatalytic oxidation of ethylene using computational fluid
413 dynamics. *CHEMICAL ENGINEERING JOURNAL* 263, 325–335.
414 <https://doi.org/10.1016/j.cej.2014.11.017>

415 Fan, W., Chan, K.Y., Zhang, C., Zhang, K., Ning, Z., Leung, M.K.H., 2018. Solar
416 photocatalytic asphalt for removal of vehicular NO_x: A feasibility study. *Applied
417 Energy* 225, 535–541. <https://doi.org/10.1016/j.apenergy.2018.04.134>

418 Faraldos, M., Kropp, R., Anderson, M.A., Sobolev, K., 2016. Photocatalytic
419 hydrophobic concrete coatings to combat air pollution. *Catalysis Today* 259,
420 228–236. <https://doi.org/10.1016/j.cattod.2015.07.025>

421 Fluent, A., 2009. 12.0 Theory Guide. Ansys Inc 5.

422 Folli, A., Strøm, M., Madsen, T.P., Henriksen, T., Lang, J., Emenius, J., Klevebrant,

423 T., Nilsson, Å., 2015. Field study of air purifying paving elements containing
424 TiO₂. *Atmospheric Environment* 107, 44–51.
425 <https://doi.org/10.1016/j.atmosenv.2015.02.025>

426 Fresno, F., Portela, R., Suárez, S., Coronado, J.M., 2014. Photocatalytic materials:
427 Recent achievements and near future trends. *Journal of Materials Chemistry A* 2,
428 2863–2884. <https://doi.org/10.1039/c3ta13793g>

429 García-yea, J.S., Torres-jardón, R., Barrera-huertas, H., Castro, T., Peralta, O., García,
430 M., 2018. Characterization of NO_x -O_x relationships during daytime
431 interchange of air masses over a mountain pass in the Mexico City megalopolis.
432 *Atmospheric Environment* 177, 100–110.
433 <https://doi.org/10.1016/j.atmosenv.2017.11.017>

434 Guo, M.Z., Ling, T.C., Poon, C.S., 2017. Photocatalytic NO_x degradation of concrete
435 surface layers intermixed and spray-coated with nano-TiO₂: Influence of
436 experimental factors. *Cement and Concrete Composites* 83, 279–289.
437 <https://doi.org/10.1016/j.cemconcomp.2017.07.022>

438 Han, B.S., Baik, J.J., Kwak, K.H., Park, S.B., 2018. Large-eddy simulation of reactive
439 pollutant exchange at the top of a street canyon. *Atmospheric Environment* 187,
440 381–389. <https://doi.org/10.1016/j.atmosenv.2018.06.012>

441 Hang, J., Luo, Z., Wang, X., He, L., Wang, B., Zhu, W., 2017. The influence of street
442 layouts and viaduct settings on daily carbon monoxide exposure and intake
443 fraction in idealized urban canyons. *Environmental Pollution* 220, 72–86.

444 <https://doi.org/10.1016/j.envpol.2016.09.024>

445 Hao, C., Xie, X., Huang, Y., Huang, Z., 2019. Study on Influence of viaduct and noise
446 barriers on the particulate matter dispersion in street canyons by CFD Modeling.
447 Atmospheric Pollution Research. <https://doi.org/10.1016/j.apr.2019.07.003>

448 Jelle Roegiers, 2018. CFD- and radiation field modeling of a gas phase photocatalytic
449 multi-tube reactor. Chemical Engineering Journal 287–299.

450 Jiang, Q., Qi, T., Yang, T., Liu, Y., 2019. Ceramic tiles for photocatalytic removal of
451 NO in indoor and outdoor air under visible light. Building and Environment 158,
452 94–103. <https://doi.org/10.1016/j.buildenv.2019.05.014>

453 Kikumoto, H., Ooka, R., 2012. A study on air pollutant dispersion with bimolecular
454 reactions in urban street canyons using large-eddy simulations. Journal of Wind
455 Engineering and Industrial Aerodynamics 104–106, 516–522.
456 <https://doi.org/10.1016/j.jweia.2012.03.001>

457 Kwak, K.H., Baik, J.J., Lee, K.Y., 2013. Dispersion and photochemical evolution of
458 reactive pollutants in street canyons. Atmospheric Environment 70, 98–107.
459 <https://doi.org/10.1016/j.atmosenv.2013.01.010>

460 Lasek, J., Yu, Y.H., Wu, J.C.S., 2013. Removal of NO_x by photocatalytic processes.
461 Journal of Photochemistry and Photobiology C: Photochemistry Reviews 14, 29–
462 52. <https://doi.org/10.1016/j.jphotochemrev.2012.08.002>

463 Lira, J.D.O.B., Padoin, N., Vilar, V.J.P., Soares, C., 2018. Photocatalytic NO_x
464 abatement : Mathematical modeling , CFD validation and reactor analysis.

465 Journal of Hazardous Materials 0–1.
466 <https://doi.org/10.1016/j.jhazmat.2018.07.009>

467 Macphee, D.E., Folli, A., 2016. Photocatalytic concretes — The interface between
468 photocatalysis and cement chemistry. *Cement and Concrete Research* 85, 48–54.
469 <https://doi.org/10.1016/j.cemconres.2016.03.007>

470 Mendoza, J.A., Lee, D.H., Kang, J.H., 2017. Photocatalytic removal of gaseous
471 nitrogen oxides using WO₃/TiO₂ particles under visible light irradiation: Effect
472 of surface modification. *Chemosphere* 182, 539–546.
473 <https://doi.org/10.1016/j.chemosphere.2017.05.069>

474 Mills, A., Hunte, S. Le, 1997. An overview of semiconductor photocatalysis. *Journal*
475 *of Photochemistry and Photobiology A: Chemistry* 108, 1–35.
476 <https://doi.org/10.1126/science.12.296.346-a>

477 Moradpour, M., Afshin, H., Farhanieh, B., 2017. A numerical investigation of
478 reactive air pollutant dispersion in urban street canyons with tree planting.
479 *Atmospheric Pollution Research* 8, 253–266.
480 <https://doi.org/10.1016/j.apr.2016.09.002>

481 Mothes, F., Ifang, S., Gallus, M., Golly, B., Boréave, A., Kurtenbach, R., Kleffmann,
482 J., George, C., Herrmann, H., 2018. Bed flow photoreactor experiments to assess
483 the photocatalytic nitrogen oxides abatement under simulated atmospheric
484 conditions. *Applied Catalysis B: Environmental* 231, 161–172.
485 <https://doi.org/10.1016/j.apcatb.2018.03.010>

486 Muilwijk, C., Schrijvers, P.J.C., Wuerz, S., Kenjereš, S., 2016. Simulations of
487 photochemical smog formation in complex urban areas. *Atmospheric*
488 *Environment* 147, 470–484. <https://doi.org/10.1016/j.atmosenv.2016.10.022>

489 Muñoz, V., Casado, C., Suárez, S., Sánchez, B., Marugán, J., 2019. Photocatalytic
490 NO_x removal: Rigorous kinetic modelling and ISO standard reactor simulation.
491 *Catalysis Today* 326, 82–93. <https://doi.org/10.1016/j.cattod.2018.09.001>

492 National Bureau of Statistics of China, 2019. *China Statistical Yearbook*, National
493 Bureau of Statistics of China.

494 National Ministry of Ecology and Environment of China, 2018. *China Vehicle*
495 *Environmental Management Annual Report*.

496 Notario, A., Bravo, I., Adame, J.A., Díaz-de-Mera, Y., Aranda, A., Rodríguez, A.,
497 Rodríguez, D., 2012. Analysis of NO, NO₂, NO_x, O₃ and oxidant (OX=O
498 3+NO₂) levels measured in a metropolitan area in the southwest of Iberian
499 Peninsula. *Atmospheric Research* 104–105, 217–226.
500 <https://doi.org/10.1016/j.atmosres.2011.10.008>

501 Passalía, C., Alfano, O.M., Brandi, R.J., 2011. Modeling and Experimental
502 Verification of a Corrugated Plate Photocatalytic Reactor Using Computational
503 Fluid Dynamics 9077–9086. <https://doi.org/10.1021/ie200756t>

504 Ryerson, T.B., Williams, E.J., Fehsenfeld, F.C., 2000. An efficient photolysis system
505 for fast-response NO₂ measurements. *Journal of Geophysical Research*
506 *Atmospheres* 105, 26447–26461. <https://doi.org/10.1029/2000JD900389>

507 Salvado, I., 2007. Two-Dimensional Modeling of a Flat-Plate Photocatalytic Reactor
508 for Oxidation of Indoor Air Pollutants 7489–7496.
509 <https://doi.org/10.1021/ie070391r>

510 Salvado, I., Hargreaves, D.M., 2007. Evaluation of the Intrinsic Photocatalytic
511 Oxidation Kinetics of Indoor Air Pollutants 41, 2028–2035.
512 <https://doi.org/10.1021/es061569o>

513 Seinfeld, J.H., 2007. Global Atmospheric Chemistry of Reactive Hydrocarbons.
514 Reactive Hydrocarbons in the Atmosphere 293–319.
515 <https://doi.org/10.1016/b978-012346240-4/50009-6>

516 Sini, J.F., Anquetin, S., Mestayer, P.G., 1996. Pollutant dispersion and thermal effects
517 in urban street canyons. *Atmospheric Environment* 30, 2659–2677.
518 [https://doi.org/10.1016/1352-2310\(95\)00321-5](https://doi.org/10.1016/1352-2310(95)00321-5)

519 Tokode, O., Prabhu, R., Lawton, L.A., Robertson, P.K.J., 2017. Journal of
520 Environmental Chemical Engineering A photocatalytic impeller reactor for gas
521 phase heterogeneous photocatalysis. *Journal of Environmental Chemical
522 Engineering* 5, 3942–3948. <https://doi.org/10.1016/j.jece.2017.07.068>

523 Vezzoli, M., Farrell, T., Baker, A., Psaltis, S., Martens, W.N., Bell, J.M., 2013.
524 Optimal catalyst thickness in titanium dioxide fixed film reactors : Mathematical
525 modelling and experimental validation. *Chemical Engineering Journal* 234, 57–
526 65. <https://doi.org/10.1016/j.cej.2013.08.049>

527 Xie, X., Zhu, Z., 2018. Effects of Heat Intensity and Inflow Wind on the Reactive

528 Pollution Dispersion in Urban Street Canyon. Journal of Shanghai Jiaotong
529 University (Science) 23, 109–116. <https://doi.org/10.1007/s12204-018-2030-x>

530 Yang, L., Hakki, A., Zheng, L., Jones, M.R., Wang, F., Macphee, D.E., 2019.
531 Photocatalytic concrete for NO_x abatement: Supported TiO₂ efficiencies and
532 impacts. Cement and Concrete Research 116, 57–64.
533 <https://doi.org/10.1016/j.cemconres.2018.11.002>

534 Yu, Q.L., Ballari, M.M., Brouwers, H.J.H., 2010. Indoor air purification using
535 heterogeneous photocatalytic oxidation. Part II: Kinetic study. Applied Catalysis
536 B: Environmental 99, 58–65. <https://doi.org/10.1016/j.apcatb.2010.05.032>

537 Zhang, W., 2014. Experimental studies on automobile exhaust photocatalytic
538 degradation on Asphalt pavement Material. Chang'an University.

539 Zheng, B., Tong, D., Li, M., Liu, F., Hong, C., Geng, G., Li, H., Li, X., Peng, L., Qi,
540 J., Yan, L., Zhang, Y., Zhao, H., Zheng, Y., He, K., Zhang, Q., 2018. Trends in
541 China's anthropogenic emissions since 2010 as the consequence of clean air
542 actions. Atmospheric Chemistry and Physics 18, 14095–14111.
543 <https://doi.org/10.5194/acp-18-14095-2018>

544